# Superfluid-insulator transition in the disordered two-dimensional Bose-Hubbard model

Fei Lin, Erik S. Sørensen, and D. M. Ceperley

Phys. Rev. B **84**, 094507 — Published 13 September 2011

DOI: 10.1103/PhysRevB.84.094507

# The superfluid-insulator transition in the disordered two-dimensional Bose-Hubbard model

Fei Lin *,[1] Erik S. Sørensen,[2] and D. M. Ceperley[1]

[1]*Department of Physics, University of Illinois at Urbana-Champaign, Urbana, IL 61801, USA*
[2]*Department of Physics and Astronomy, McMaster University, Hamilton, Ontario, Canada L8S 4M1*

(Dated: August 22, 2011)

We investigate the superfluid-insulator transition in the disordered two-dimensional Bose-Hubbard model through quantum Monte Carlo simulations. The Bose-Hubbard model is studied in the presence of site disorder and the quantum critical point between the Bose-glass and superfluid is determined in the grand canonical ensemble at $\mu/U = 0$ (close to $\rho = 0.5$), $\mu/U = 0.375$ (close to $\rho = 1$), and $\mu/U = 1$ as well as in the canonical ensemble at $\rho = 0.5$ and 1. Particular attention is paid to disorder averaging and it is shown that a large number of disorder realizations is needed in order to obtain reliable results. Typically, more than 100,000 disorder realizations was used. In the grand canonical ensemble we find $Zt_c/U = 0.112(1)$ with $\mu/U = 0.375$, significantly different from previous studies. When compared to the critical point in the absence of disorder ($Zt_c/U = 0.2385$), this result confirms previous findings showing that disorder enlarges the superfluid region. At the critical point we then study the dynamic conductivity.

PACS numbers: 61.43.Bn, 05.60.Gg, 05.70.Jk, 02.70.Ss

## I. INTRODUCTION

Since the publication of seminal papers on superfluid-insulator transition by Fisher *et al.* ,[1,2] the disordered two-dimensional (2D) Bose-Hubbard (BH) model has attracted much theoretical attention. The disordered BH model with Cooper pairs acting as charge-2$e$ bosons has been argued to describe the superconductor-insulator transition in thin amorphous films.[2–5] Recently, with the development of experimental techniques for constructing the BH model by confining cold alkali atoms in optical lattices, superfluid (SF) to Mott insulator (MI) transitions have been observed in clean optical lattices[6]. Further experiments have introduced disorder in the optical lattices by speckle fields to investigate the phase diagram of a disordered three dimensional optical lattice[7,8]. Although experimental techniques still need to be refined, there is renewed interest in the disordered BH model from experiment. From theory, there is a long-standing research interest in studying the disorder induced phase transitions and searching for Bose glass (BG) phase.[9–31] In particular, recent work has focused on the transition in 3 dimensions[27,31–33] and the validity of the relation $z = d$ established by Fisher et al.[1] has been questioned both in numerical[34,35] and theoretical studies[36]. Here we shall focus exclusively on the disordered two-dimensional (2D) model where a number of outstanding questions remain.

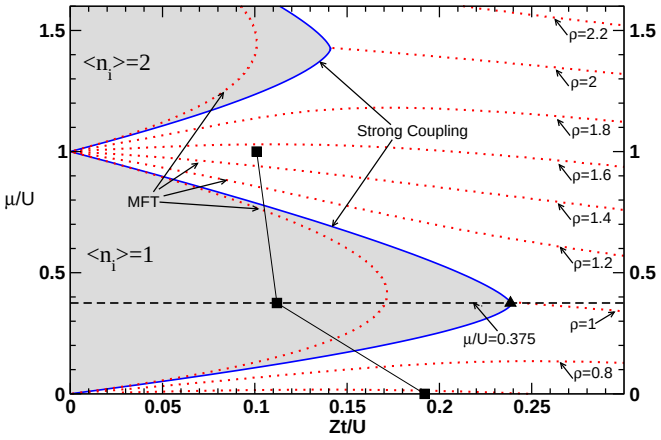


FIG. 1: (Color online) The phase diagram of the 2$D$ Bose-Hubbard model. Shaded areas are the Mott-insulating phases for zero disorder as determined from strong coupling expansions in Ref. 37,38. The mean field phase boundaries and constant density profiles for zero disorder are shown as red dotted lines. The dashed line indicates the constant chemical potential $\mu/U = 0.375$. ▲ indicates the location of the transition to the Mott phase in the *absence* of disorder as determined by SSE simulations along the dashed line from Ref 39. The three ■'s from bottom up are for the locations of superfluid to Bose glass transitions in the *presence* of disorder at $\mu/U = 0, 0.375, 1$, respectively, as determined from SSE simulations in the present work.

The disordered 2D BH Hamiltonian is given by

$$H = -t\sum_{i,\delta}(a^\dagger_{i+\delta}a_i + \text{H.c.}) + \frac{U}{2}\sum_i n_i(n_i-1) + \sum_i(\epsilon_i-\mu)n_i, \quad (1)$$

where $\delta = \hat{\mathbf{x}}, \hat{\mathbf{y}}$, $t$ is the nearest neighbor hopping amplitude, $a^\dagger_i(a_i)$ is a boson creation (annihilation) opera-

*Current address: Department of Physics, Robeson Hall, Virginia Tech, Blacksburg, VA 24061-0435, USA

tor, H.c. means Hermitian conjugate, $n_i = a_i^\dagger a_i$ is the number operator, $U$ is on-site interaction, $\mu$ is chemical potential and $\epsilon_i$ is uniformly distributed in the interval $[-\Delta, \Delta]$, with $\Delta$ controlling the disorder strength. Hereafter, we shall explicitly give energy values for both $t$ and $U$ in each calculation to facilitate comparisons with calculations in the literature, since Hamiltonian definitions in each paper may be different. The phase diagram for this model in the absence of disorder as determined from strong coupling expansions (from Ref. 37,38) is shown in Fig. 1 with Mott insulating lobes with fixed on-site particle number extending into the superfluid phase. The mean field phase diagram[40] is shown as dotted lines in Fig. 1 and the importance of fluctuations is clearly evident from the discrepancy between the mean field and strong coupling results at the tip of the envelopes. Despite its relative simplicity, a detailed understanding of this model with disorder has proven surprisingly difficult in particular for numerical work.

Existing studies using various methods address different aspects of the disordered BH model, and often arrive at contradicting conclusions. It is therefore most useful to revisit this problem using current high performance numerical techniques. In the presence of disorder it is known[1] that a BG phase appears in addition to the SF and MI phase present without disorder. The question of whether a transition directly from the SF to the MI without an intermediate BG phase is possible in the presence of disorder arises. However, this question now seems settled with a proof that there is always an intermediate BG phase.[30] In the simulations we report here we are always in the strong disorder regime ($\Delta = U$) and we focus on the SF-BG transition since we expect the MI phases to be strongly suppressed at strong disorder.

A model closely related to the Bose-Hubbard model is the (N=2) quantum rotors model: $(\cos(\theta_{\mathbf{r}}), \sin(\theta_{\mathbf{r}}))$, believed to be in the same universality class as Eq. (1). This model describes a wide range of phase transitions dominated by phase-fluctuations:

$$H_{\rm qr} = \frac{U}{2}\sum_{\mathbf{r}}\left(\frac{1}{i}\frac{\partial}{\partial\theta_{\mathbf{r}}}\right)^2 + i\sum_{\mathbf{r}}\mu\frac{\partial}{\partial\theta_{\mathbf{r}}} - t\sum_{\langle\mathbf{r},\mathbf{r}'\rangle}\cos(\theta_{\mathbf{r}} - \theta_{\mathbf{r}'}). \tag{2}$$

Here, $t$ is the renormalized hopping strength and $\frac{1}{i}\frac{\partial}{\partial\theta_{\mathbf{r}}} = L_{\mathbf{r}}$ is the angular momentum of the quantum rotor. The angular momentum can be thought of as describing the deviation of the particle number from its mean, $L_{\mathbf{r}} \simeq n_{\mathbf{r}} - n_0$. This model can be obtained from Eq. (1) if amplitude fluctuations are integrated out when compared to Eq. (1). It is implicitly assumed that only phase-fluctuations are important at the quantum critical point (QCP) while amplitude fluctuations are neglected. The model Eq. (2) can be simulated very efficiently using the Villain (link-current) representation and a specialized directed geometrical worm algorithm[24,25] has been developed for this purpose. This technique can be applied to both the clean and disordered model and high precision results can be obtained. However, when compared to results obtained by direct simulations of Eq. (1) by Batrouni *et al.* [41] as well as from simulations of Eq. (1) in the hard-core limit by Makivić *et al.* [34], discrepancies appeared in particular for the universal features of the conductivity at the critical point, as we discuss below. Here we shall show that a likely explanation for these discrepancies is an inaccurate determination of the QCP in the direct simulations of Eq. (1). Furthermore, it is important, from our point of view, to provide accurate quantum critical parameter values (e.g. $t_c$ and $U_c$ for the Hamiltonian defined in Eq. (1)) using recently improved simulation techniques.

Our calculations proceed under two different conditions: fixed particle number (canonical) in order to follow the calculations of Ref. 41 or fixed chemical potential (grand canonical). This corresponds to taking two different routes in probing QCP in the BH model phase diagram illustrated by the dotted and dashed lines in Fig. 1. Previous calculations on the *clean* system by Šmakov *et al.*[39] using a quantum Monte Carlo (QMC) method have located the QCP at $Zt_c/U = 0.2385$ (solid triangle in Fig. 1) at $\mu/U = 0.375$ (equivalent to $\rho = 1$), where $Z = 4$ is the coordination number for the square lattice. As evident from Fig. 1 this is in excellent agreement with the strong-coupling result from Ref. 37,38. Here we follow a similar approach to determine the QCP but with an added on-site *disordered* chemical potentials $\epsilon_i \in [-\Delta, \Delta]$, with $\Delta = U$ in the region of strong disorder.

At the critical point in a 2D system, the DC conductivity was predicted[2] to have a universal value, $\sigma^*$, close to the conductivity "quantum" $\sigma_Q = e^{\star 2}/h$, with $e^\star$ the charge of the bosons. However, the exact universal value has yet to be determined. Experiments[3,4] suggest the DC conductivity value to be a little larger than $\sigma_Q$ but there are concerns that the experimental temperature (typically $> 0.5$ K) is not low enough. Using the quantum rotor model, Eq. (2), Sørensen *et al.*[11] showed that the universal conductivity value is given by $\bar{\sigma}^* = (0.14 \pm 0.01)\sigma_Q$. Previously, exact diagonalization on a hard-core BH model by Runge[42] gave a value of $\bar{\sigma}^* = (0.15 \pm 0.01)\sigma_Q$ in good agreement. Later, by doing world-line quantum Monte Carlo (WLQMC) simulations directly on a disordered 2D BH model, Batrouni *et al.*[41] found $\bar{\sigma}^* = (0.45 \pm 0.07)\sigma_Q$ and Makivić *et al.* [34] found $\bar{\sigma}^* = (1.2 \pm 0.2)\sigma_Q$ using a hard-core BH model. These calculations differ from each other and the experimental value. It was later pointed out[43] that in $d$ spatial dimensions, the dynamic conductivity $\sigma(\omega)$ obeys the following scaling relation near the QCP

$$\sigma(\omega) = 2\pi\sigma_Q\left(\frac{k_B T}{\hbar c}\right)^{(d-2)/z}\Sigma\left(\frac{\hbar\omega}{k_B T}\right), \tag{3}$$

which might in part explain the difference between the experimental value and numerical calculations since the $\hbar\omega/k_B T \to 0$ is achieved in the experiments while in the imaginary-time QMC simulations with Matsubara frequency $\omega_k$ one always has $\hbar\omega_k/k_B T = 2\pi k > 1$. The

regimes $\hbar\omega/(k_BT) \ll 1$ and $\hbar\omega/(k_BT) \gg 1$ are dominated by different transport mechanisms, hydrodynamic-collision dominated and collisionless phase-coherent, respectively. Hence, there is little reason to believe that a simple extrapolation using only $\hbar\omega/k_BT \gg 1$ can correctly determine the observed experimental DC conductivity. If a careful extrapolation first to $L \to \infty$ and then $T \to 0$ is performed it is possible to gain some information about this limit.[39] Nevertheless, the entire function $\Sigma$ in Eq. (3) is universal and the above mentioned numerical results should still agree on this universal function and the extrapolations should yield the same number. However, that extrapolated number which we shall call $\bar{\sigma}^*$ might not be closely related to the DC conductivity but will instead correspond to a higher frequency part of $\Sigma$. A sketch of the expected behavior is shown in Fig. 2. Our results here show that if a careful determination of the QCP is performed, Eq. (1) and Eq. (2) yield the same value for $\bar{\sigma}^*$.

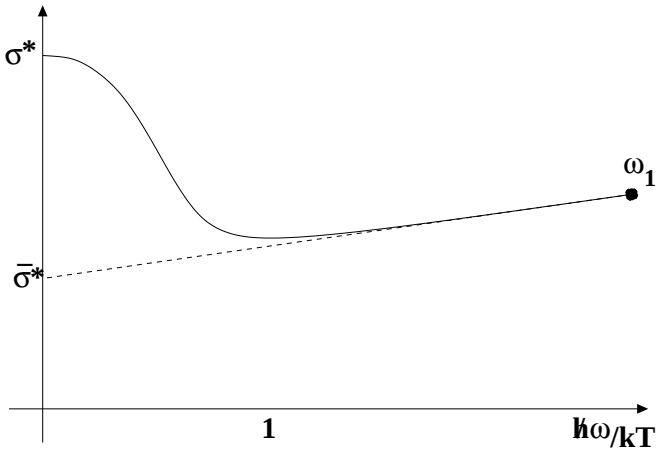


FIG. 2: A sketch of the conductivity with the two regimes, $\hbar\omega/(k_BT) \gg 1$ and $\hbar\omega/(k_BT) \ll 1$ clearly apparent. Also shown is the difference between the universal DC conductivity $\sigma^*$ and the conductivity $\bar{\sigma}^*$ obtained from extrapolating the high-frequency numerical data. An approximate position of the first non-zero Matsubara frequency is also shown.

If the conductivity for the BH model at the critical point is a scaling function of $\hbar\omega/k_BT$ one would expect plots of $\sigma(\omega)$ versus $\omega$ to show *deviations* from scaling at the critical point even for finite systems. A primary goal of this paper is to see if such deviations are observable for the two-dimensional disordered BH model if the QCP is determined carefully. We believe that the results we present here show clear indications of such deviations from scaling with $\omega$.

Not only the conductivity value and dynamic conductivity scaling differ in historical studies, but also the QCP has diverse estimates. For example, Zhang *et al.*[44] used both ground state and finite temperature QMC simulations to locate the QCP of a hard-core BH model, which seems to agree with earlier work of Krauth, Trivedi and Ceperley.[10] These two simulations are, however, quite different from what Batrouni *et al.* found[41]. It is noteworthy that these QMC calculations have used only about 100 disorder samples; we show below that this is not sufficient for a precise determination of the critical point.

Recently, QMC algorithms for the BH model have undergone a big improvement in efficiency with the development of stochastic series expansion (SSE) algorithm[45] and the directed loop update technique.[46,47] This algorithm does not have the imaginary-time discretization error inherent in the traditional WLQMC method. The loop updates are especially important in the quantum critical region where the long correlation time substantially increases the errors of the WLQMC simulations. It is now feasible to check the convergence of measured quantities with the disorder averaging by increasing the number of disorder samples dramatically. This has been found by Wallin *et al.*[13] and Hitchcock *et al.*[27] to be crucial in order to obtain reliable results.

In this paper, we first discuss the SSE algorithm as it is applied to the BH model. In particular, we discuss the measurement of superfluid density and dynamic conductivity. Then tests on the equilibration process and autocorrelation functions of the simulations are described to validate the estimates of the superfluid density needed to locate the QCP. We then show the superfluid density scaling figures for both the canonical and grand canonical ensembles, discussing the connection and differences from previous results. Finally, we show dynamical conductivity scaling and the extrapolated universal conductivity values in the high frequency limit.

## II. NUMERICAL METHOD AND CONVERGENCE TESTS

As pointed out by Weichman,[26] analytic solutions of the model, Eq. (1), based on perturbation of the non-interacting limit has a fundamental difficulty because in the absence of repulsive interaction $U$ or the Pauli exclusion for fermions, the presence of any disorder no matter how weak will condense a macroscopic number of particles into the lowest localized free particle eigenstate of the random potential. This is not a meaningful state to do perturbation on. When the interaction $U$ is non-zero, a complicated competition between the interaction and disorder potential makes it impossible to do analytic calculations. In this paper, we resort to QMC simulations of the model with the SSE algorithm,[45–47], since it is able to treat any interaction strength and disorder realization. The method is briefly discussed below.

In the SSE formalism, the above site representation of Hamiltonian Eq. (1) needs to be written in a bond representation.

$$H = -\sum_{b=1}^{N_b}(H_{1b} + H_{2b}) \tag{4}$$

where the $b = \langle ij \rangle$ is the bond index, $H_{1b}$ is a diagonal operator, and $H_{2b}$ is an off-diagonal operator given by the following equations:

$$\begin{aligned} H_{1,b} &= C - [\frac{\tilde{U}}{2} n_i(n_i - 1) + \frac{\tilde{U}}{2} n_j(n_j - 1) + (\tilde{\epsilon}_i - \tilde{\mu})n_i \\ &\quad + (\tilde{\epsilon}_j - \tilde{\mu})n_j], \\ H_{2,b} &= t(a_i^\dagger a_j + H.c.), \end{aligned} \tag{5}$$

where $\tilde{A} = A/Z$, with $A$ one of $\mu, \epsilon_i, U$ and $Z = 4$ being the coordination number of each lattice site. $N_b = ZN/2$ is number of bonds in the system with $N$ lattice sites. $C$ is a constant chosen to ensure a positive definite expansion. Since $\tilde{\epsilon}$ is a random number, we need to use the disorder amplitude $\Delta$ in order to determine an appropriate value for the constant $C$.

The partition function can then be expanded as

$$\begin{aligned} Z &= \mathrm{Tr}\{e^{-\beta H}\} = \sum_\alpha \sum_{n=0}^{\infty} \frac{(-\beta)^n}{n!} \langle \alpha | H^n | \alpha \rangle, \\ &= \sum_\alpha \sum_{n=0}^{\infty} \sum_{S_n} \frac{\beta^n}{n!} \langle \alpha | \prod_{i=1}^{n} H_{a_i,b_i} | \alpha \rangle, \end{aligned} \tag{6}$$

where $\{|\alpha\rangle\}$ represents a complete state basis and

$$S_n = [a_1, b_1], [a_2, b_2], \ldots, [a_n, b_n]$$

is an operator-bond sequence, with $a_i \in \{1, 2\}$ denoting the type of operator (1=diagonal, 2=off-diagonal), and $b_i \in \{1, \ldots, N_b\}$ being the bond index. The expansion is now truncated at order $M$, and $M - n$ unit operators for the $n$th order term are inserted:

$$Z = \sum_\alpha \sum_{S_M} \frac{\beta^n (M - n)!}{M!} \langle \alpha | \prod_{i=1}^{n} H_{a_i,b_i} | \alpha \rangle. \tag{7}$$

Here $M$ has been made large enough so that the probability for the expansion order exceeding $M$ can be neglected. The Monte Carlo weight for the configuration $(\alpha, S_M)$ is then given by:

$$w(\alpha, S_M) = \frac{\beta^n (M - n)!}{M!} \langle \alpha | \prod_{i=1}^{n} H_{a_i,b_i} | \alpha \rangle. \tag{8}$$

The resulting configuration space, consisting of state and operator sequences, is updated with both diagonal and loop updates.

The diagonal update probability with $n \to n \pm 1$ is given by

$$\begin{aligned} P(n \to n + 1) &= \frac{N_b \beta \langle \alpha(p) | H_{1,b} | \alpha(p) \rangle}{M - n}, \\ P(n \to n - 1) &= \frac{M - n + 1}{N_b \beta \langle \alpha(p) | H_{1,b} | \alpha(p) \rangle} \end{aligned} \tag{9}$$

where $|\alpha(p)\rangle$ is the propagated state

$$|\alpha(p)\rangle \sim \prod_{i=1}^{p} H_{a_i,b_i} |\alpha\rangle. \tag{10}$$

For the loop update, transition probabilities during the loop construction is chosen to have bounce-free or bounce minimizing solutions of the operator vertex equation.[47] The configuration weights for operator vertex in the disordered BH model are, for particle occupation $n_i$ and $n_j$ for nearest neighbor $\langle ij \rangle$, given by the following different cases:

$$\begin{aligned} &w(n_i, n_j; n_i + 1, n_j - 1) = t_{ij} \sqrt{(n_i + 1) n_j} (1 - \delta_{n_i, n_{\max}}) \\ &w(n_i, n_j; n_i - 1, n_j + 1) = t_{ij} \sqrt{n_i (n_j + 1)} (1 - \delta_{n_j, n_{\max}}) \\ &w(n_i, n_j; n_i, n_j) = C - [\frac{\tilde{U}}{2} n_i(n_i - 1) + \frac{\tilde{U}}{2} n_j(n_j - 1) \\ &+ (\tilde{\epsilon}_i - \tilde{\mu})n_i + (\tilde{\epsilon}_j - \tilde{\mu})n_j]. \end{aligned} \tag{11}$$

Here $n_{\max}$ is the maximum number of bosons that can occupy the same site. $n_{\max}$ is usually assigned a large enough value (compared with the average density of the system) so that it can allow particle number fluctuations while at the same time will never actually be exceeded during the QMC simulations. From the operator vertex weight expressions, we can see that for the disordered BH model, all these weights need to be calculated "on the fly". Note that we have not explored the possibility of tabulating all the operator vertex weights, which could speedup the calculation. In the tabulation, one would need to set up $ZN/2$ probability tables (each table corresponds to one bond); the number of elements in the table is determined by $n_{\max}$, e.g. for $n_{\max} = 4$, each table has 3392 elements.

The total energy of the system is related to the expansion order of the operator sequence

$$E = -\frac{\langle n \rangle}{\beta}, \tag{12}$$

where $n$ is number of non-unit operators in the operator sequence as discussed above.

The physical quantity that indicates the superfluid-insulator transition is the normalized superfluid density $\rho_s$,[48] computed as the average square winding numbers $\langle W^2 \rangle$

$$\rho_s = \frac{\langle W^2 \rangle}{2t\beta\rho}, \tag{13}$$

where $W^2 = W_x^2 + W_y^2$, $\beta$ is inverse temperature, and $\rho$ is the average number of particles per lattice site.

To locate QCP, we will use the normalized superfluid density finite-size scaling relation[49]

$$\rho_s = L^\alpha f(aL^{1/\nu}\delta, \beta L^{-z}), \tag{14}$$

where $L$ is the linear dimension of the square lattice, $d = 2$ is lattice dimension, $\alpha = 2 - d - z$, $\delta$ measures the distance to the critical point (e.g., to determine $U_c$, we have $\delta = (U - U_c)/U_c$, and similarly for $t_c$), $z$ is dynamical exponent, which is predicted[2] to be $z = 2$, $a$ is a non-universal metric number, and the function $f$ is universal.

Hence, we have $\alpha = -2$, and if we keep $\beta L^{-z}$ fixed, and plot $L^2\rho_s$ versus $Zt/U$ for different lattice sizes, all the curves will intersect at the critical value of $U_c$. Note that we assume the validity of the relation $z = d$ which has been brought into question recently.[36]

The conductivity of the BH model as a function of Matsubura frequency $\omega_k = 2\pi k/(\hbar\beta)$ can be calculated from the linear response relations (we illustrate using the $x$ direction; similar response formula apply for the $y$ direction)[50–52]

$$\sigma(i\omega_k) = 2\pi\sigma_Q \frac{\langle k_x\rangle - \Lambda_{xx}(i\omega_k)}{\omega_k}, \tag{15}$$

where $\langle k_x\rangle$ is kinetic energy per link along the $x$ direction, and $\Lambda_{xx}(i\omega_k)$ is the Fourier transform of the imaginary-time current-current correlation function $\Lambda_{xx}(\tau)$

$$\Lambda_{xx}(i\omega_k) = \frac{1}{N}\int_0^\beta d\tau e^{i\omega_k\tau}\Lambda_{xx}(\tau). \tag{16}$$

Here $N$ is total number of lattice sites, and $\Lambda_{xx}(\tau) = \langle j_x(\tau)j_x(0)\rangle$, with the paramagnetic current being given by $j_x(0) = it\sum_{\mathbf{r}}(a^\dagger_{\mathbf{r}+x}a_{\mathbf{r}} - a^\dagger_{\mathbf{r}}a_{\mathbf{r}+x})$, and $j_x(\tau)$ being the Heisenberg representation of $j_x(0)$. Note that the smallest Matsubara frequency $\omega_1$ corresponds to $\hbar\omega_1/(k_BT) = 2\pi$ significantly larger than one. Hence, as pointed out by Damle *et al.* [43] this type of imaginary-time QMC calculation will necessarily be in the the collisionless phase coherent regime with $\hbar\omega/(k_BT) \gg 1$. In the following we set $\hbar = 1$.

To calculate the imaginary-time current-current correlation function $\Lambda_{xx}(\tau)$, we follow the discussion of Ref. 39 and divide $\Lambda_{xx}(\tau)$ into four components (which may be thought of as combinations of current and anti-current terms) by

$$\Lambda_{xx}(\tau) = \sum_{\gamma,\nu=\pm}\Lambda^{\gamma\nu}_{xx}(\tau), \tag{17}$$

and

$$\Lambda^{\gamma\nu}_{xx}(\tau) = \sum_{\mathbf{r}}\langle K^\gamma_x(\mathbf{r},\tau)K^\nu_x(\mathbf{0},0)\rangle, \tag{18}$$

$$K^+_x(\mathbf{r},\tau) = ta^\dagger_{\mathbf{r}+x}(\tau)a_{\mathbf{r}}(\tau), \tag{19}$$

$$K^-_x(\mathbf{r},\tau) = -ta^\dagger_{\mathbf{r}}(\tau)a_{\mathbf{r}+x}(\tau). \tag{20}$$

Finally the imaginary-time current-current correlation function can be calculated with a binomial summation in QMC simulations[39,45]

$$\Lambda_{xx}(i\omega_k) = \sum_{\gamma,\nu=\pm}\Lambda^{\gamma\nu}_{xx}(\tau), \\ = \sum_{\mathbf{r};\gamma,\nu=\pm}\langle\frac{1}{\beta}\sum_{m=0}^{n-2}a_{mn}(i\omega_k)N(\nu,\gamma;m)\rangle, \tag{21}$$

where $a_{mn}(i\omega_k)$ is the degenerate hypergeometric (Kummer) function,[53] i.e., $a_{mn}(i\omega_k) = {}_1F_1(m+1,n;i\beta\omega_k)$, $N(\nu,\gamma;m)$ is the number of times the operators $K^\gamma_x$ and $K^\nu_x$ appear in the SSE operator sequence separated by $m$ operators, and $n$ is the expansion order. The virtue of the above formulation is that the imaginary-time integral in Eq. (16) is performed analytically, hence eliminating the discretization error of the imaginary-time integral that is present in the conventional WLQMC.[41]

### 1. Convergence Tests

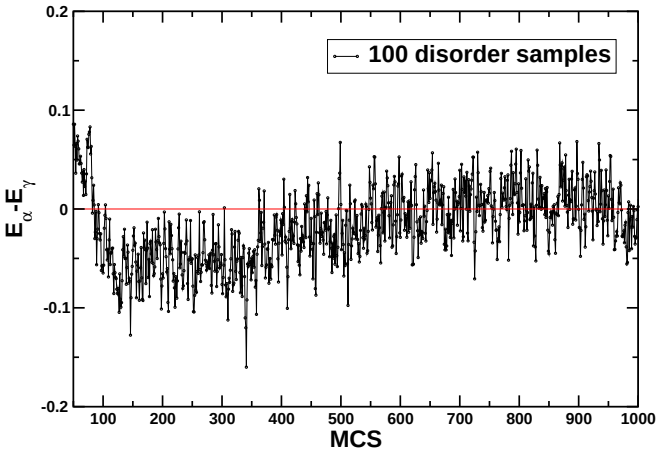


FIG. 3: The energy difference between two replicas $E_\alpha - E_\gamma$ as a function of MCS averaged over 100 disorder samples. Results are shown for $L = 16$, $t = 0.5$, $U = 11$, and $\beta = 12.8$. We start recording the energy difference after 50 MCS.

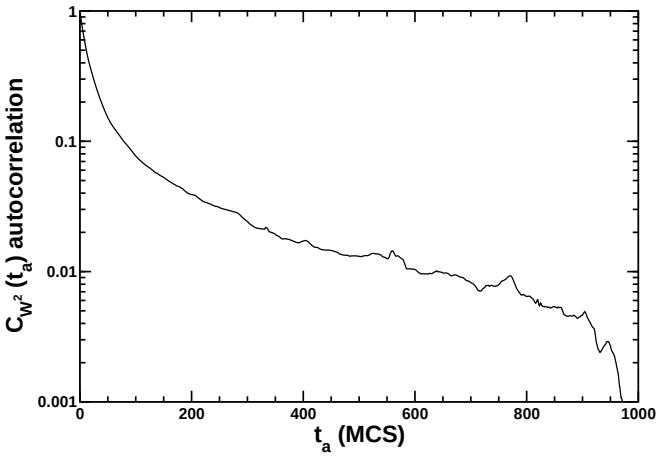


FIG. 4: The autocorrelation function, $C_{W^2}(t_a)$, for $W^2$ averaged over 100 disorder samples for $L = 16$, $t = 0.5$, $U = 11$, and $\beta = 12.8$. Note that the $y$-axis is on a log scale.

Numerically we perform SSE simulations for lattice sizes $L = 6, 8, 10, 12, 16$. According to scaling relation Eq. (14), the corresponding inverse temperatures for

these lattices are $\beta = 1.8, 3.2, 5.0, 7.2, 12.8$, leading to a constant $\beta L^{-2} = 0.05$. Our strategy is to ensure that each disorder realization has been equilibrated, resulting in a few statistically independent measurements for each disorder realization, with the error-bars then obtained from the disorder averaging where each realization can be considered statistically independent. We have performed several tests to ensure that this equilibration is attained and that the number of disorder realizations are sufficient[27].

We begin by considering the equilibration of the energy between two different replicas with the *same* disorder realization. We define one Monte Carlo sweep (MCS) as 1 diagonal update, which includes a sweep through all diagonal operators in the SSE expansion, followed by 10 loop updates (the number of loop updates included in 1 MCS is arbitrary, but it is usually determined by the ratio of the SSE expansion order to the average loop length). In Fig. 3, we show the equilibration of the energy difference between two energy replicas as a function of MCS for $L = 16$, $t = 0.5$, $U = 11$ averaged over 100 disorder realizations. As mentioned, replica simulation means that for each disorder realization, we start two parallel SSE simulations $\alpha$ and $\gamma$ with vastly different initial configurations but with the *same* disorder realization, and monitor the evolution of $E_\alpha - E_\gamma$. We see that after about 500 MCS, $E_\alpha - E_\gamma$ fluctuates around zero, showing equilibration.

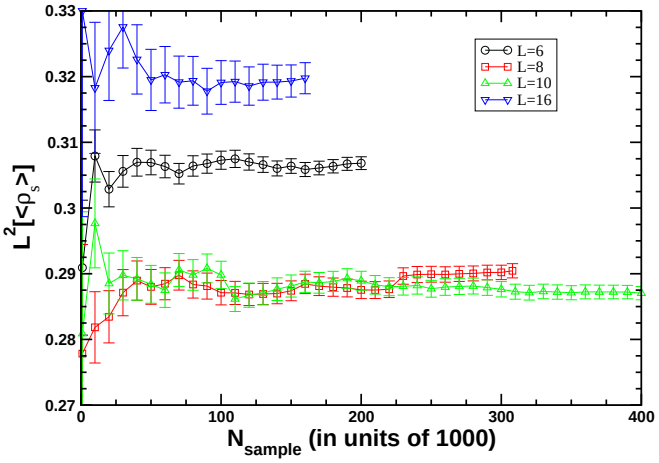


FIG. 5: (Color online) Convergence of the superfluid density for $t = 0.5$ and $U = 11$ as a function of the number of disorder samples $N_{\rm sample}$ for various lattice sizes, $L = 6, 8, 10$, and 16.

We then proceed check the convergence of the winding number $W^2$ by calculating its autocorrelation function,

$$C_{W^2}(t_a) = \frac{\langle W^2(0)W^2(t_a)\rangle - \langle W^2\rangle^2}{\langle W^4\rangle - \langle W^2\rangle^2}. \qquad (22)$$

Our results for $C_{W^2}(t_a)$ versus $t_a$ (MCS) are shown in Fig. 4 on a log scale averaged over 100 disorder samples. Since we expect the leading term in $C_{W^2}(t_a)$ to scale as $e^{-t_a/\tau}$, we estimate the autocorrelation time to be around $\tau \sim 40$ MCS.

Based on the above tests we set the following parameters for the SSE simulations and measurements: for each disorder realization we perform 1000 MCS to warm up the system, which is followed by 1000 MCS measurements with each measurement being separated by 1 MCS. While this might seem inadequate to obtain small error bars for a single disorder realization, this approach is in fact optimal since each disorder realization is statistically independent; reliable error-bars can then be obtained from the disorder averaging. We have done tests for the worst case, i.e., longest warm-up MCS and $W^2$ autocorrelation time for $L = 16$, $t = 0.5$, $U = 11$, and $\beta = 12.8$, so we expect the parameters to be sufficient for the other lattice settings.

Finally, we focus on the disorder averaging which we denote by $[\cdot]$ to distinguish it from thermal averages $< \cdot >$. Often one finds that the estimate of a quantity one wishes to calculate obeys a rather broad distribution with a substantial tail[27] with a difference between the average and the most likely values. This will be reflected in an underestimation of the error-bar calculated from the standard deviation and a slow "movement" of the average as the number of disorder realizations is increased with the error-bar essentially constant with respect to the number of averages. We check our convergence here by focusing on the behavior of the superfluid density as we increase the number of disorder samples $N_{\rm sample}$. See Fig. 5. For each curve in the figure, the first point is for 1,000 disorder realizations, the second for 10,000 disorder realizations, and for subsequent points, the increment is 10,000 disorder samples. It is important to note that 1,000 disorder realizations is already *an order of magnitude more* than the previous calculations,[10,41,44] where the number of disorder realizations was taken to be around 100. Here, we find that 1,000 disorder samples is still far from convergence. The idea of self-averaging does not seem to apply here, either. For the remainder of our results we have used in excess of 100,000 disorder realizations to ensure reliable results.

## III. RESULTS

### A. Fixed particle number, $\rho = 0.5$, 1

As described, the SSE is essentially a grand canonical simulation algorithm and suitable for fixed chemical potential QMC simulations. However, in order to be as close as possible to previous calculations by Batrouni *et al.* ,[41] we also want to do simulations with fixed particle number for each disorder realization. It is possible to forbid particle number fluctuation during the loop construction,[54,55] but we will adopt a simpler approach. We first do some rough estimates of chemical potentials to yield total particle number close to the required value for a set of disorder realizations. We then use the average chemical potential for all disorder realizations in the construction of the probability table during the loop update,

and reject any closed loops that change the total particle number. In practice, we find that with the roughly estimated chemical potential the loss of efficiency caused by additional rejection is insignificant, typically 5% more rejection than the grand canonical simulations.

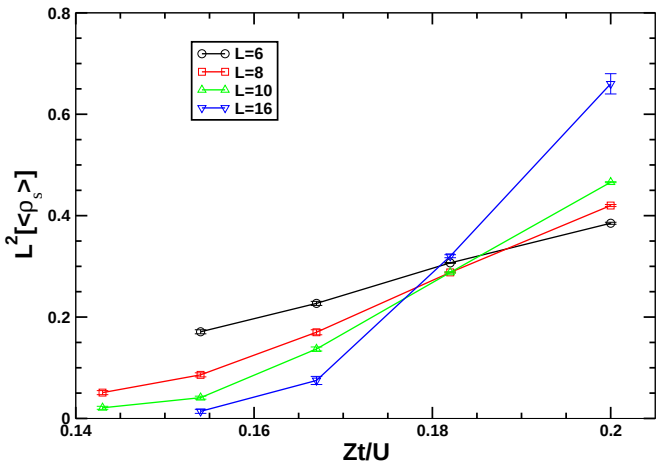


FIG. 6: (Color online) Superfluid density scaling from canonical simulations, i.e., fixed particle number with density $\rho = 0.5$, for $\Delta = 12$ and $t = 0.5$, for various lattice sizes, $L = 6, 8, 10$, and 16.

We now turn to our results using SSE simulations in the canonical ensemble with $n_{\max} = 4$, fixed particle density $\rho = 0.5$, and fixed disorder strength $\Delta = 12$ and hopping integral $t = 0.5$, which are the same as in Ref. 41. Note that canonical systems with fixed particle density of $\rho = 0.5$ are very close to the grand canonical systems with $\mu/U = 0$. A series of $U$ values will be used in the simulations to search for the critical point $U_c$ based on finite-size scaling relation for the normalized superfluid density Eq. (14).

To locate the QCP $U_c$ or equivalently $Zt/U_c$, we plot in Fig. 6 the superfluid density $L^2\rho_s$ as a function of $Zt/U$ (fixing $t = 0.5$ and using a $U$ grid of $U = 11, 12, 13$, and 14) for various lattice sizes $L = 6, 8, 10$, and 16. All 4 curves intersect very close to the point $Zt/U_c = 0.182$. The crossing of the curves is not as "perfect" as for the clean system where larger system sizes can be simulated and it would appear that corrections to scaling for the smallest size $L = 6$ might be sizable. However, for disordered systems the results in Fig. 6 is at par with the best one can obtain. We also note that the fact that we do obtain a crossing of the curves at a single point is an indirect validation of the scaling relation Eq.(14) with $z = d$. Based on the data shown in Fig. 6, we estimate the critical point to be $Zt/U_c = 0.182 \pm 0.003$ or $U_c = 11.0 \pm 0.5$. To achieve a more accurate result will remain a challenge for some time. Since canonical simulations with $\rho = 0.5$ correspond closely to the grand canonical simulations with $\mu/U = 0$, we can compare the QCP obtained in these two simulations, and find that this canonical QCP value for $\rho = 0.5$ is very close to the grand canonical value of $(Zt/U)_c = 0.192$ at $\mu/U = 0$, which is shown as black square at the bottom of Fig. 1.

The same QCP in Ref. 41 (note factor of $t/2$ instead of $t$ in their Hamiltonian) was estimated to be $(U/t)_c \sim 7$, substantially different from the result we obtain here[56]. However, for $\rho = 0.75$ Ref. 10 (note factor of $t/2$ instead of $t$ in their Hamiltonian) finds $(U/t)_c \sim 10$ and in the hard-core limit Ref. 44 (note factor of $U$ in stead of $U/t$ in their Hamiltonian) finds $(U/t)_c = 9.9 \pm 0.4$ with $\rho = 0.5$ in reasonable agreement with our results. We note that in Ref. 41 the location of the QCP was obtained partly by requiring the frequency dependent conductivity, $\sigma(\omega)$, to scale with $\omega$ at the critical point in violation of Eq. (3). We now turn to a discussion of our results for the dynamic conductivity.

As discussed above, the dynamic conductivity calculated with Matsubara frequency is expected to satisfy the scaling relation Eq. (3). The implication of this scaling law for numerical simulations is that $\sigma(\omega, T, L)$ in the limit $L \to \infty$ as $T$ approaches 0 should be a function of a single variable $\hbar\omega/(k_B T)$. Therefore, if the dynamic conductivity curves calculated from different lattice sizes are plotted versus $\omega$, one would expect deviations from a single curve to be visible at the smallest Matsubara frequencies since finite size dependence there is likely the smallest and the data should be close to scaling with $\hbar\omega/(k_B T)$ even without extrapolation to $L \to \infty$. See also Ref. 39. Such behavior is clearly visible in Fig. 7, where SSE results for the dynamic conductivity $\sigma(\omega_k)/\sigma_Q$ at the critical point $Zt/U_c = 0.182$ are shown. All curves from 4 different lattice sizes overlap with each other at high frequency limit but differ at the low frequency side. A rough estimate of the high frequency universal conductivity, $\bar{\sigma}^*$ using the lattice size $L = 16$ gives $\bar{\sigma}^* \sim 0.17\sigma_Q$. This is in surprisingly good agreement with simulations

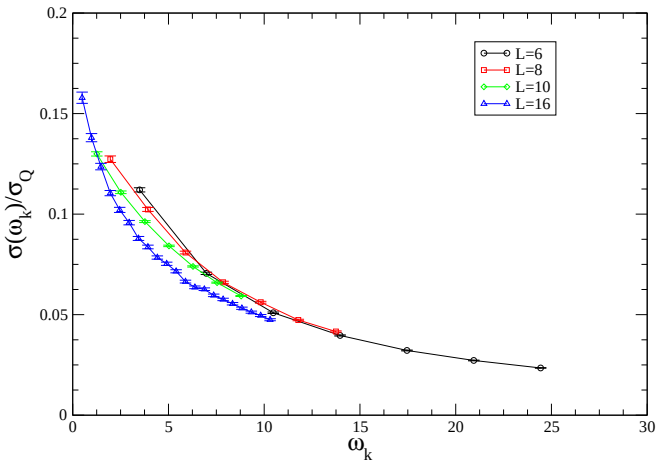


FIG. 7: (Color online) Dynamic conductivity scaling plot $\sigma(\omega_k)/\sigma_Q$ vs Matsubara frequency $\omega_k$ for $Zt/U_c = 0.182$ and $t = 0.5$.

of the quantum rotor model, Eq. (2), where one finds $\bar{\sigma}^* = (0.14 \pm 0.01)\sigma_Q$, [11] as well as with the exact di-

agonalization result $(0.15 \pm 0.01)\sigma_Q$ for a hard-core BH model,[42] as one would expect for a universal quantity. However, this value is much less than the value found by Batrouni *et al.* $(0.47 \pm 0.08)\sigma_Q$.[41] The discrepancy could be due to an inaccurate estimate of the QCP in Ref. 41 obtained partly by assuming that $\sigma(\omega)$ should scale with $\omega$ at the quantum critical point.

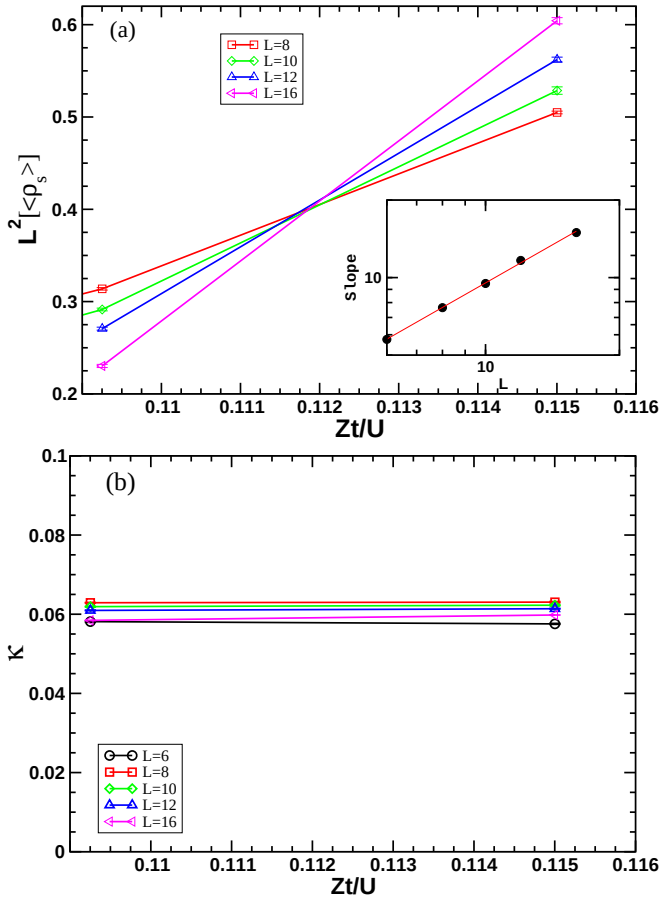


FIG. 8: (Color online). (a) Scaling curves of the superfluid density from grand canonical simulations at $\mu/U = 0.375$. The inset shows the slope of these curves at the QCP on a log-log scale. (b) The compressibility $\kappa$ in the same region.

In addition we have performed canonical simulations with $\rho = 1$, and determined the QCP at $[(Zt/U)_c = 0.108(2)]$, which is slightly different from the fixed chemical potential $(\mu/U = 0.375)$ analysis value of $(Zt/U)_c = 0.112(1)$ to be discussed in the next section.

### B. Grand Canonical Simulations $\mu/U = 0, 0.375, 1$

Close to the commensurate filling of $\rho = 1$ corresponding to $\mu/U = 0.375$ the QCP has been determined in Ref. 39 for the *clean* BH model (see also solid triangle in Fig. 1). Here we are interested in further investigating the effect of disorder on this transition by keeping all the other parameters the same as in Ref. 39 while setting the disorder potential amplitude $\Delta = U$.

Note that in generating the disordered onsite potential $\epsilon_i$ for the system, we make sure that the average of the disordered onsite potential $\sum_i \epsilon_i/N = 0$ for each disordered configuration of the system. This can be achieved by first generating a disorder configuration and calculating the average of the disordered potential, then subtracting this average from the generated potential at each lattice site.

Our results are shown in Fig. 8(a) where $L^2[< \rho_s >]$ is plotted for different system sizes close to the QCP. The scaling law here is the same as outlined above for the simulations in the canonical ensemble and again we note that the relation $z = d$ was assumed. As can be seen from Fig. 8(a) the curves cross very nearly in a single point and it is easy to estimate the corresponding QCP points as $(Zt/U)_c = 0.112(1)$. Very interestingly, when this is compared to the results for the clean system QCP of $(Zt/U)_c = 0.2385$ from Ref. 39, it is clear that the introduction of disorder at this commensurate filling has enhanced the superfluid region. The QCP with (■) and without (▲) disorder at $\mu/U = 0.375$ are shown along the dashed line in Fig. 1. A similar indication for disorder-enhanced superfluidity has been found by Krauth *et al.* ,[10] but the effect is even more noticeable in our results.

Also shown in Fig. 8(b) (as an inset) is the slope of $L^2\rho_s$ at the QCP. From the scaling relation Eq. (14) it is clear that this slope should scale with $L^{1/\nu}$. The solid line in the inset is a fit to the data yielding $\nu \sim 1$ in agreement with the quantum version of the Harris criterion $\nu \geq 2/d$.

In Fig. 8(b) are shown results for the compressibility, $\kappa$, through the QCP. As can be seen, the compressibility remains constant through the QCP. It is expected that in the presence of disorder the compressibility will scale as $\kappa \sim \delta^{\nu(d-z)}$. The fact that our results for $\kappa$ remain constant through the transition is consistent with the relation $z = d$, although it does not rule out $z < d$.

At the QCP we also measure the dynamic conductivity with grand canonical QMC simulations, shown in Fig. 9. Like the simulations in the canonical ensemble, we observe that the data appear to scale with $\omega_k$ at high frequency but very clearly deviate from this behavior at low frequencies. Again we emphasize that this is consistent with $\sigma(\omega)$ scaling with $\hbar\omega/(k_B T)$ rather than $\omega$. Here we can also attempt to estimate $\bar{\sigma}^*$ and we find it to be around $0.17\sigma_Q$, in very good agreement with the results for the canonical simulations from the previous section as well as with the simulations of the quantum rotor model.[11] As before, we note that the universal conductivity, $\bar{\sigma}^*$ estimated here and in the previous section corresponds to the conductivity value in the high frequency limit, not the DC conductivity measured experimentally.

We have also performed simulations at $\mu/U = 1$ where we find $(Zt/U)_c = 0.101$ as well as for $\mu/U = 0$ where we find $(Zt/U)_c = 0.192$. These QCPs are also shown as solid black squares in Fig. 1.

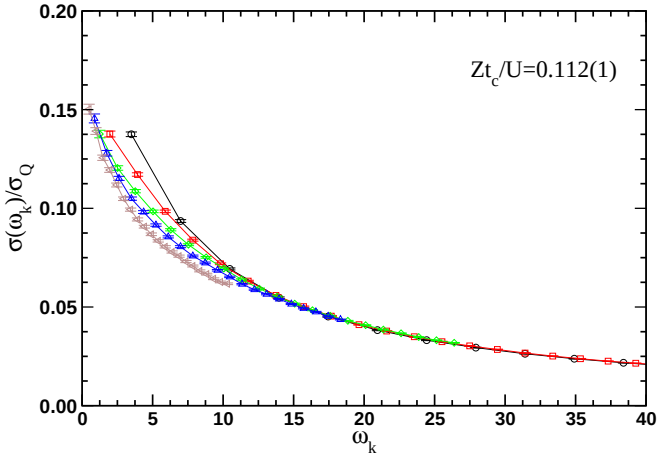


FIG. 9: (Color online) Dynamic conductivity $\sigma(\omega_k)/\sigma_Q$ vs Matsubara frequency $\omega_k$ for $Zt_c/U = 0.112$ in a disordered grand canonical system at $\mu/U = 0.375$.

## IV. CONCLUSION

In this paper we have determined the superfluid-insulator transition QCPs of the 2D BH model with strong disorder for both commensurate $\rho = 1$ and incommensurate $\rho = 0.5$ systems. In connection with previous calculations in the literature we have identified the disorder-induced superfluidity at $\rho = 1$ in an otherwise Mott insulating region in the clean limit. Our main results are summarized in Fig. 1 where the dramatic results of disorder are clearly visible. While in the past, high precision results have been available for the quantum rotor model as well as the BH model in the hard-core limit, the results we present here are among the first simulations of the full BH model with large disorder. Our results clearly indicate that these 3 models in the presence of disorder are in the same universality class.

At the QCP, we also compute the dynamic conductivity as a function of the Matsubara frequency. The universal conductivity at high frequency limit is estimated to be around $0.17\sigma_Q$ in good agreement with previous calculations on quantum rotor models.[11] Most notably, at the QCP, the dynamic conductivity shows clear deviations from scaling with $\omega$, consistent instead with the expected scaling with $\omega/(k_BT)$. In addition, we checked in detail the convergence with the number of disorder realizations finding that a large number of disorder realizations (usually on the order of $10^4$) is necessary to have a fully convergent superfluid density value. This implies that some previous calculations in the literature with disorder realizations of the order of $10^2$, might not be reliable. This has allowed us to determine the QCP for several values of $\mu/U$ for the disordered Bose-Hubbard model.

## V. ACKNOWLEDGMENTS

We would like to acknowledge useful correspondence with G. Batrouni, R. Scalettar, and J. Šmakov. We also thank H. Monien for permission to use data from Ref. 37,38. FL was supported by the US Department of Energy under award number DE-FG52-06NA26170 when this study was carried out. ESS is supported by the Natural Sciences and Engineering Research Council of Canada and the Canadian Foundation for Innovation. DMC was supported by the DARPA OLE program. Computation time was provided by the SHARCNET and NCSA supercomputing facilities.

[1] M. P. A. Fisher, P. B. Weichman, G. Grinstein, and D. S. Fisher, Phys. Rev. B **40**, 546 (1989).
[2] M. P. A. Fisher, G. Grinstein, and S. M. Girvin, Phys. Rev. Lett. **64**, 587 (1990).
[3] D. B. Haviland, Y. Liu, and A. M. Goldman, Phys. Rev. Lett. **62**, 2180 (1989).
[4] H. M. Jaeger, D. B. Haviland, B. G. Orr, and A. M. Goldman, Phys. Rev. B **40**, 182 (1989).
[5] M. C. Cha, M. P. A. Fisher, S. M. Girvin, M. Wallin, and A. P. Young, Phys. Rev. B **44**, 6883 (1991).
[6] M. Greiner, O. Mandel, T. Esslinger, T. W. Hansch, and I. Bloch, Nature **415**, 39 (2002).
[7] M. White et al., Phys. Rev. Lett. **102**, 055301 (2009).
[8] M. Pasienski, D. McKay, M. White, and B. DeMarco, Nature Physics **6**, 677 (2010).
[9] R. T. Scalettar, G. G. Batrouni, and G. T. Zimanyi, Phys. Rev. Lett. **66**, 3144 (1991).
[10] W. Krauth, N. Trivedi, and D. Ceperley, Phys. Rev. Lett. **67**, 2307 (1991).
[11] E. S. Sørensen, M. Wallin, S. M. Girvin, and A. P. Young, Phys. Rev. Lett. **69**, 828 (1992).
[12] K. G. Singh and D. S. Rokhsar, Phys. Rev. B **46**, 3002 (1992).
[13] M. Wallin, E. S. Sørensen, S. M. Girvin, and A. P. Young, Phys. Rev. B **49**, 12115 (1994).
[14] R. V. Pai, R. Pandit, H. R. Krishnamurthy, and S. Ramasesha, Phys. Rev. Lett. **76**, 2937 (1996).
[15] R. Mukhopadhyay and P. B. Weichman, Phys. Rev. Lett. **76**, 2977 (1996).
[16] J. K. Freericks and H. Monien, Phys. Rev. B **53**, 2691 (1996).
[17] B. V. Svistunov, Phys. Rev. B **54**, 16131 (1996).
[18] I. F. Herbut, Phys. Rev. Lett. **79**, 3502 (1997).
[19] J. Kisker and H. Rieger, Phys. Rev. B **55**, R11981 (1997).
[20] F. Pazmandi and G. T. Zimanyi, Phys. Rev. B **57**, 5044 (1998).
[21] I. F. Herbut, Phys. Rev. B **57**, 13729 (1998).
[22] P. Sen, N. Trivedi, and D. M. Ceperley, Phys. Rev. Lett. **86**, 4092 (2001).
[23] J.-W. Lee, M.-C. Cha, and D. Kim, Phys. Rev. Lett. **87**, 247006 (2001).
[24] F. Alet and E. S. Sørensen, Phys. Rev. E **67**, 015701 (2003).
[25] F. Alet and E. S. Sørensen, Phys. Rev. E **68**, 026702

(2003).
[26] P. B. Weichman, Mod. Phys. Lett. **22**, 2623 (2008).
[27] P. Hitchcock and E. S. Sørensen, Phys. Rev. B **73**, 174523 (2006).
[28] J. Wu and P. Phillips, Phys. Rev. B **78**, 014515 (2008).
[29] U. Bissbort and W. Hofstetter, Europhys. Lett. **86**, 50007 (2009).
[30] L. Pollet, N. V. Prokof'ev, B. V. Svistunov, and M. Troyer, Phys. Rev. Lett. **103**, 140402 (2010).
[31] F. Kruger, J. Wu, and P. Phillips, Phys. Rev. B **80**, 094526 (2009).
[32] B. Capogrosso-Sansone, N. V. Prokofev, and B. V. Svistunov, Phys. Rev. B **75**, 134302 (2007).
[33] V. Gurarie, L. Pollet, N. V. Prokofev, B. V. Svistunov, and M. Troyer, Phys. Rev. B **80**, 214519 (2009).
[34] M. Makivić, N. Trivedi, and S. Ullah, Phys. Rev. Lett. **71**, 2307 (1993).
[35] A. Priyadarshee, S. Chandrasekharan, J.-W. Lee, and H. U. Baranger, Phys. Rev. Lett. **97**, 115703 (2006).
[36] P. B. Weichman and R. Mukhopadhyay, Phys. Rev. Lett. **98**, 245701 (2007).
[37] N. Elstner and H. Monien, Physical Review B **59**, 12184 (1999).
[38] M. Niemeyer, J. K. Freericks, and H. Monien, Physical Review B **60**, 2357 (1999).
[39] J. Šmakov and E. Sørensen, Phys. Rev. Lett. **95**, 180603 (2005).
[40] F. Alet and E. S. Sørensen, Phys. Rev. B **70**, 024513 (2004).
[41] G. G. Batrouni, B. Larson, R. T. Scalettar, J. Tobochnik, and J. Wang, Phys. Rev. B **48**, 9628 (1993).
[42] K. J. Runge, Phys. Rev. B **45**, 13136 (1992).
[43] K. Damle and S. Sachdev, Phys. Rev. B **56**, 8714 (1997).
[44] S. Zhang, N. Kawashima, J. Carlson, and J. E. Gubernatis, Phys. Rev. Lett. **74**, 1500 (1995).
[45] A. W. Sandvik, J. Phys. A: Math. Gen. **25**, 3667 (1992).
[46] A. W. Sandvik, Phys. Rev. B **59**, R14157 (1999).
[47] O. F. Syljuasen and A. W. Sandvik, Phys. Rev. E **66**, 046701 (2002).
[48] E. L. Pollock and D. M. Ceperley, Phys. Rev. B **36**, 8343 (1987).
[49] V. Privman and M. E. Fisher, Phys. Rev. B **30**, 322 (1984).
[50] D. J. Scalapino, S. R. White, and S. C. Zhang, Phys. Rev. Lett. **68**, 2830 (1992).
[51] D. J. Scalapino, S. R. White, and S. C. Zhang, Phys. Rev. B **47**, 7995 (1993).
[52] G. D. Mahan, *Many-Particle Physics* (2nd ed., Plenum Press, New York, 1990).
[53] M. Abramowitz and I. A. Stegun, *Handbook of Mathematical Functions with Formulas, Graphs, and Mathematical Tables* (9th ed., Dover, New York, 1964).
[54] S. Rombouts, K. V. Houcke, and L. Pollet, Phys. Rev. Lett. **96**, 180603 (2006).
[55] K. V. Houcke, S. Rombouts, and L. Pollet, Phys. Rev. E **73**, 056703 (2006).
[56] Due to possible differences in the definition of the hopping term it is possible that their critical point $(U/t)_c = 7$ in our units should be $(U/t)_c = 14$. G. Batrouni private communication.